Combining off-lattice Monte Carlo and cellular automata for the simulation of hard-sphere systems

Federico G. Pazzona,* Pierfranco Demontis, and Giuseppe B. Suffritti

Dipartimento di Chimica e Farmacia, Università degli Studi di Sassari and Consorzio Interuniversitario Nazionale per la Scienza e Tecnologia dei Materiali (INSTM), Unità di Ricerca di Sassari, via Vienna, 2, I-07100 Sassari, Italy

(Received 18 April 2014; published 28 August 2014)

In the present work we show how the update rule of a diffusive cellular automaton with mutual exclusion can be exploited in off-lattice Monte Carlo simulations of hard spheres to obtain a synchronous Monte Carlo sampling that satisfies the detailed balance principle.

DOI: 10.1103/PhysRevE.90.023307 PACS number(s): 05.10.Ln, 07.05.Tp, 47.11.Qr

I. INTRODUCTION

Due to their remarkable physical properties [1,2], hard-sphere models of fluids cover a primary role in statistical mechanics from both the theoretical [3] and the computational point of view [4,5]. A number of methods were developed to simulate hard-sphere systems more efficiently than the local Metropolis method [6–8], and parallelization schemes were proposed to run hard-sphere Monte Carlo (MC) simulations on parallel architectures (see Anderson *et al.* [9], and references therein). In such methods, space decomposition techniques are used to avoid overlaps, which can arise from the synchronous movement of more than one particle (atom or molecule).

In the present work we show how the updating rule of a synchronous cellular automaton (CA) [10–15] for mutually exclusive particles [16,17] can replace the role of space decomposition in the MC updating of hard-sphere configurations, producing a synchronous MC algorithm.

Our algorithm shares with the work of Anderson *et al.* [9] the tessellation of the space enclosed within the simulation box by means of a three-dimensional grid of adjacent cubes, which we call *cells*. However, in our work the spheres are allowed to leave their parent cells during every single MC step, and a further tessellation of the physical space enclosed within every cell into a number of *sites* is used to determine the destination position of every moving sphere within the available space only.

II. OFF-LATTICE AND LATTICE SPACE

In order to proceed with the description of the algorithm, we need to define the (off-lattice) simulation space and its discrete (lattice) counterpart. For simplicity, we consider a cubic space, $\mathcal{V}$, of volume $V = L^3$ ranging from 0 to $L \in \mathbb{R}$ in each one of the x, y, and z directions and enclosing N hard spheres of diameter σ. The N spheres are allowed to occupy any position in $\mathcal{V}$ provided that one sphere does not overlap another. Periodic boundary conditions are assumed.

The lattice counterpart of the simulation space $\mathcal{V}$ is the homogeneous lattice $\mathcal{L}$, defined as

$$\mathcal{L} = \{\mathbf{c}_1, \ldots, \mathbf{c}_{z^3}\}, \tag{1}$$

made of z *cells* per side of the simulation box (z is an integer number) and containing, therefore, z^3 cells each of side $\ell = L/z$ and volume $v = \ell^3$. In Eq. (1) the (cubic) cells are labeled by their centers, $\mathbf{c}_k$, with $k = 1, \ldots, z^3$.

Every cell communicates with a limited number of cells, which constitute the *cell neighborhood*. The neighborhood is the same for every cell (due to lattice homogeneity), and includes a different number of cells depending on whether the Von Neumann (VN) or the Moore (M) neighborhood is used [11]. The notation $\mathcal{N}_{\mathrm{VN}}(\mathbf{c})$ and $\mathcal{N}_{\mathrm{M}}(\mathbf{c})$ will be used to indicate the Von Neumann and the Moore neighborhood, respectively, of the cell centered at the position $\mathbf{c} \in \mathcal{L}$. The cell $\mathbf{c}$ itself is not included in the definition of $\mathcal{N}_{\mathrm{X}}(\mathbf{c})$ (with X = VN, M). In Table I we provide an accurate description of the two types of neighborhood, whereas in Figs. 1(a) and 1(b) the Von Neumann and Moore neighborhoods are represented (2D projection).

III. BOUNDARY LATTICE

According to Table I, the distance vectors $\mathbf{c} + \widehat{\mathbf{v}}_j$, $j = 1, \ldots, 6$, indicate the relative positions of the six first neighbors of cell $\mathbf{c}$, constituting the Von Neumann neighborhood of cell $\mathbf{c}$. The center of every *boundary* between $\mathbf{c}$ and each of such neighbors is then located at the position $\mathbf{c} + \frac{1}{2}\widehat{\mathbf{v}}_j$, $j = 1, \ldots, 6$, and it is called *boundary site*. Given that there are z^3 cells in the cubic lattice $\mathcal{L}$, we have that the *boundary lattice*, defined as

$$\begin{aligned}\mathcal{B} &= \{\mathbf{b}_1, \mathbf{b}_2, \mathbf{b}_3, \ldots, \mathbf{b}_{3z^3-2}, \mathbf{b}_{3z^3-1}, \mathbf{b}_{3z^3}\} \\ &= \left\{ \mathbf{c}_1 + \frac{1}{2}\begin{pmatrix}\ell\\0\\0\end{pmatrix}, \mathbf{c}_1 + \frac{1}{2}\begin{pmatrix}0\\\ell\\0\end{pmatrix}, \mathbf{c}_1 + \frac{1}{2}\begin{pmatrix}0\\0\\\ell\end{pmatrix} \right. \\ &\quad \left. , \ldots, \mathbf{c}_{z^3} + \frac{1}{2}\begin{pmatrix}\ell\\0\\0\end{pmatrix}, \mathbf{c}_{z^3} + \frac{1}{2}\begin{pmatrix}0\\\ell\\0\end{pmatrix}, \mathbf{c}_{z^3} + \frac{1}{2}\begin{pmatrix}0\\0\\\ell\end{pmatrix} \right\}, \end{aligned} \tag{2}$$

is made of $3z^3$ boundary sites, and we say that the six boundary sites located at positions

$$\mathbf{c}_k \pm \frac{1}{2}\begin{pmatrix}\ell\\0\\0\end{pmatrix}, \quad \mathbf{c}_k \pm \frac{1}{2}\begin{pmatrix}0\\\ell\\0\end{pmatrix}, \quad \mathbf{c}_k \pm \frac{1}{2}\begin{pmatrix}0\\0\\\ell\end{pmatrix} \tag{3}$$

enclose the cell $\mathbf{c}_k$.

Let us now define the neighborhood of a boundary site. Whereas the boundary lattice described above makes use of the Von Neumann neighborhood *only* (i.e., it does not change whether the Von Neumann or the Moore neighborhood is used

*fpazzona@uniss.it

TABLE I. The Von Neumann and the Moore neighborhoods for a three-dimensional grid of cells (the superscript T indicates the transpose). Given a cell centered at $\mathbf{r}_c$, the set of neighbors is given, respectively, by $\{\mathbf{c}+\widehat{\mathbf{v}}_1,\ldots,\mathbf{c}+\widehat{\mathbf{v}}_6\}$ or $\{\mathbf{c}+\widehat{\mathbf{u}}_1,\ldots,\mathbf{c}+\widehat{\mathbf{u}}_{26}\}$, depending on whether the Von Neumann or the Moore neighborhood is used.

Von Neumann neighborhood, $\mathcal{N}_{\rm VN}$			
$\widehat{\mathbf{v}}_1^T,\ldots,\widehat{\mathbf{v}}_6^T :=$	$(\pm\ell,0,0)$	$(0,\pm\ell,0)$	$(0,0,\pm\ell)$
Moore neighborhood, $\mathcal{N}_{\rm M}$			
$\widehat{\mathbf{u}}_1^T,\ldots,\widehat{\mathbf{u}}_{26}^T :=$	$(\pm\ell,0,0)$,	$(0,\pm\ell,0)$,	$(0,0,\pm\ell)$,
	$(\pm\ell,\pm\ell,0)$,	$(\pm\ell,\mp\ell,0)$,	$(\pm\ell,0,\pm\ell)$,
	$(\pm\ell,0,\mp\ell)$,	$(0,\pm\ell,\pm\ell)$,	$(0,\pm\ell,\mp\ell)$,
	$(\pm\ell,\pm\ell,\pm\ell)$,	$(\pm\ell,\mp\ell,\pm\ell)$,	$(\pm\ell,\pm\ell,\mp\ell)$,
	$(\mp\ell,\pm\ell,\pm\ell)$		

to describe the cell-to-cell connections), the neighborhood of a boundary site is sensitive to the particular type of cell neighborhood chosen for the simulation. The definition of neighborhood, $\mathcal{N}_{\mathcal{B}}(\mathbf{b})$, of the boundary site $\mathbf{b}$, assumed to be located at the center of the interface between cells $\mathbf{c}_k$ and $\mathbf{c}_{k'}$, is the following: given the cell neighborhood, $\mathcal{N}_{\rm X}$ (with X = VN or M, depending on whether the Von Neumann or the Moore neighborhood is used), $\mathcal{N}_{\mathcal{B}}(\mathbf{b})$ *includes all the boundary sites enclosing the cells contained in* $\mathcal{N}_{\rm X}(\mathbf{c}_k)$ *and* $\mathcal{N}_{\rm X}(\mathbf{c}_{k'})$. By definition, $\mathcal{N}_{\mathcal{B}}(\mathbf{b})$ turns out to contain the boundary site $\mathbf{b}$ itself. In Figs. 1(c) and 1(d), the boundary neighborhood around a boundary site is represented, respectively, in the case of Von Neumann and Moore neighborhoods (2D projection).

Finally, we indicate as $\mathbf{c}_1(\mathbf{b})$ and $\mathbf{c}_2(\mathbf{b})$ the two cells that communicate with each other through the boundary site $\mathbf{b}$. For example, if we indicate as $\mathbf{b}$ the boundary site in yellow in Figs. 1(c) and 1(d), then $\{\mathbf{c}_1(\mathbf{b}),\mathbf{c}_2(\mathbf{b})\}=\{\mathbf{c}_8,\mathbf{c}_{13}\}$.

IV. ALGORITHM

The simulation starts with a random configuration of N nonoverlapping spheres and proceeds through discrete ($k=1,2,\ldots$) MC iterations. The position of the centers of the N spheres at iteration k represents a configuration, denoted $\mathbf{R}^k=\{\mathbf{r}_1,\ldots,\mathbf{r}_N\}$. We shall describe the evolution of the system through a sequence of operations, each one represented as the action of an operator on the configuration $\mathbf{R}$. Since the algorithm does not change from one MC iteration to the other, we drop the iteration superscript k.

First of all, the operator $\mathcal{C}$ maps the configuration $\mathbf{R}$ into a coarse-grained configuration, called $\widetilde{\mathbf{R}}$, in which the position of every sphere's center is rounded to the center of the cell it falls within:

$$\mathcal{C}:\mathbf{R}\mapsto\widetilde{\mathbf{R}}:=\left\{\mathrm{INT}[\mathbf{r}_j/\ell]+\left(\tfrac{\ell}{2},\tfrac{\ell}{2},\tfrac{\ell}{2}\right)^T\right\}_{j=1,\ldots,N}=\{\widetilde{\mathbf{r}}_1,\ldots,\widetilde{\mathbf{r}}_N\},\tag{4}$$

where T indicates the transpose.

Now, we use the lattices $\mathcal{L}$ and $\mathcal{B}$ to let the spheres move while preserving the excluded volume condition. Let us suppose the system is configured as $\mathbf{R}=\{\mathbf{r}_1,\ldots,\mathbf{r}_N\}$, and let us consider the sphere j, with position $\mathbf{r}_j$, belonging to the cell ℓ_j. We introduce γ (with $0<\gamma\leqslant 1$) as the probability of sphere j (as of any other sphere) to stay at rest. As a consequence, the probability of the particle to reach one of the six boundaries around the cell $\widetilde{\mathbf{r}}_j$ reads $(1-\gamma)/6$. All the spheres pick one (or none) of their respective nearest boundaries at the same time according to such criterion. In the resulting configuration, $\mathbf{I}=\{\mathbf{i}_1,\ldots,\mathbf{i}_N\}$, which we call a *boundary configuration*, some spheres appear to have jumped from their original positions (i.e., $\mathbf{r}_j$) into the exact location of a nearest boundary (so that for such spheres $\mathbf{i}_j\neq\mathbf{r}_j$), and the other spheres did not move from their original positions (i.e., for such spheres $\mathbf{i}_j=\mathbf{r}_j$). The generation of $\mathbf{I}$ from $\mathbf{R}$ can be represented as the action of the stochastic operator $\mathcal{I}$:

$$\mathcal{I}:\mathbf{R}\mapsto\mathbf{I}\text{ with probability }p(\mathbf{I}|\mathbf{R}),\tag{5}$$

where the conditional probability of generating $\mathbf{I}$ from $\mathbf{R}$ is

$$p(\mathbf{I}|\mathbf{R})=\prod_{j=1}^{N}\left(\frac{1-\gamma}{6}\right)^{\xi_j}\gamma^{1-\xi_j},\tag{6}$$

with the boolean ξ_j indicating whether or not the sphere j jumped into a nearest boundary during the transformation $\mathbf{R}\to\mathbf{I}$; i.e., $\xi_j=1-\delta(\mathbf{r}_j-\mathbf{i}_j)$. The *occupancy* of each boundary site, $n(\mathbf{b})$, is the number of spheres that, according

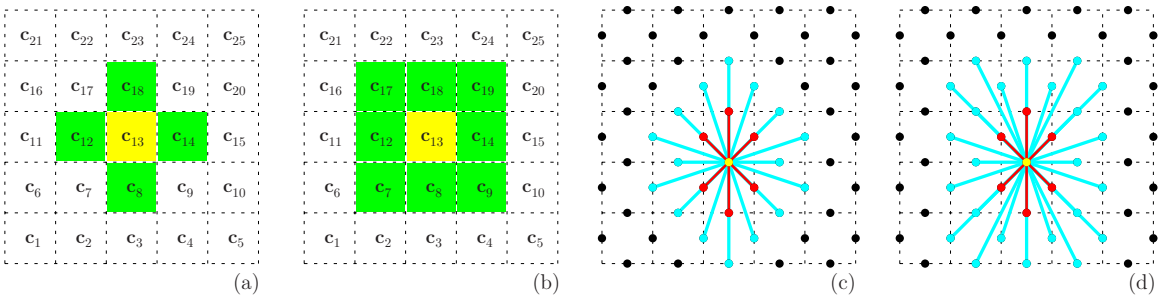

FIG. 1. (Color online) (a) A two-dimensional sketch of a small lattice of cells, numbered as $\mathbf{c}_1,\mathbf{c}_2,\ldots$. Cell $\mathbf{c}_{13}$ is enhanced in yellow, and its Von Neumann neighboring cells are in green. In (b) we sketch the same as in (a), but with the Moore neighbors of cell $\mathbf{c}_{13}$ enhanced in green. In (c) the cell-to-cell boundaries are sketched as a two-dimensional grid (filled circles). We enhanced the connections (Von Neumann neighborhood) involving the boundary (in yellow) placed in between of cells ℓ_8 and ℓ_{13}. Of such connections, the 6 pointing to the boundaries (red circles) having access to either cell ℓ_8 or cell ℓ_{13} constitute the first connection shell and are in red, whereas the 16 pointing to to the boundaries (cyan circles) having access to either the neighbors of cell ℓ_8 or the neighbors of cell ℓ_{13} constitute the second connection shell and are in cyan. In (d) the enhanced connections refer to the case of the Moore neighborhood.

to the boundary configuration $\mathbf{I}$, occupy each boundary site:

$$n(\mathbf{b}) = \sum_{j=1}^{N} \delta(\mathbf{i}_j - \mathbf{b}). \tag{7}$$

Let us assume that j reached a boundary. If other spheres occupy the same boundary or a neighboring one, there is chance for them to end up in conflicting positions. Therefore, the sphere in a boundary is driven back to its original position if, as a result of the choice made by all the spheres, the boundary occupied by j (which is $\mathbf{i}_j$) is occupied by some other sphere, and/or if any of the boundaries in the set $\mathcal{N}_{\mathcal{B}}(\mathbf{i}_j)$ is occupied. We apply such operation to all the spheres at the same time. The resulting configuration, $\mathbf{I}' = \{\mathbf{i}'_1, \ldots, \mathbf{i}'_N\}$, is another boundary configuration originated through the action of a deterministic operator $\mathcal{D}$ on $\mathbf{I}$:

$$\begin{aligned} \mathcal{D} : \mathbf{I} \mapsto \mathbf{I}' &:= \{\mathbf{r}_j + (\mathbf{i}_j - \mathbf{r}_j)\xi'_j\}_{j=1,\ldots,N} \\ &= \{\mathbf{i}'_1, \ldots, \mathbf{i}'_N\}, \end{aligned} \tag{8}$$

with

$$\xi'_j = \xi_j \Theta\left[2 - \sum_{\mathbf{b}\in\mathcal{N}_{\mathcal{B}}(\mathbf{i}_j)} n(\mathbf{b})\right], \tag{9}$$

where Θ is the Heaviside function, i.e., $\Theta[x] = 0$ if $x < 0$ and 1 otherwise.

Every sphere in a boundary site, say sphere j in $\mathbf{i}'_j$, has now access to the space enclosed within the two cells that share that boundary [i.e., $\mathbf{c}_1(\mathbf{i}'_j)$ and $\mathbf{c}_2(\mathbf{i}'_j)$], and is therefore to be considered as a *jumping sphere*. At this point, the space enclosed within these two cells is further discretized into a lattice of A sites, say $\mathcal{A}^{(j)} := \{\mathbf{a}_1^{(j)}, \ldots, \mathbf{a}_A^{(j)}\}$. The lattice $\mathcal{A}^{(j)}$ can be chosen arbitrarily. Our choice for $\mathcal{A}$ is a $2M \times M \times M$ lattice of cubes tessellating the two-cell space. In principle, any point in the space within every cube represents a possible destination of the jumping sphere. However, to minimize the jump rejectance, we operate on the lattice $\mathcal{A}^{(j)}$ in such a way as to enhance the probability of the particle to choose a position which does not cause any overlap with other spheres. Therefore, we generate the lattice $\widehat{\mathcal{A}}^{(j)} := \{\widehat{\mathbf{a}}_1^{(j)}, \ldots, \widehat{\mathbf{a}}_A^{(j)}\}$ of possible outcoming positions by operating on $\mathcal{A}^{(j)}$ as follows:

(i) We discard all the sites that have all their respective eight corners falling within a radius σ from the center of any of the spheres in the neighborhood.

(ii) We locate the site that is nearest to the position, say $\mathbf{r}_j$, occupied by the jumping sphere *before* reaching the boundary site, and we move it to a position exactly coincident with $\mathbf{r}_j$. This is a necessary step because the jumping sphere, j, must be given the chance to recover its original position to ensure detailed balance.

(iii) We move independently each of the nondiscarded sites (all except the one located at $\mathbf{r}_j$) of a random amount within their respective cube.

The resulting site positions represent the lattice $\widehat{\mathcal{A}}^{(j)}$. At this point, the notion of cubic volume associated to each site [we used such notion to determine the site corners in step (i)] is lost; i.e., every site represents merely a position in space. We derive the probability of each position in $\widehat{\mathcal{A}}^{(j)}$ to be chosen by proceeding as follows:

(iv) We assign to each position ν in the lattice $\widehat{\mathcal{A}}^{(j)}$ a statistical weight, $w_\nu^{(j)}$, equal to 1 if the distance between the νth point, located at $\widehat{\mathbf{a}}_\nu^{(j)}$, and each of the spheres in the cell containing ν and in its neighborhood is larger than σ, and equal to 0 otherwise.

(v) We choose as the outcoming position of j one site out of all those sites in set $\widehat{\mathcal{A}}^{(j)}$ that have $w_\nu^{(j)} = 1$. For a hard-spheres system, this is the same as choosing an output site, say ν, according to the probability $p_\nu^{(j)}$ defined as

$$p_\nu^{(j)} = \frac{w_\nu^{(j)}}{\sum_{\nu'} w_{\nu'}^{(j)}}. \tag{10}$$

Let us now interpret the displacement of every jumping sphere (i.e., every j such that $\xi'_j = 1$) from its original position (i.e., $\mathbf{r}_j$) to a new one (i.e., $\mathbf{a}_\nu^{(j)}$, with $\nu \in [1, A] \in \mathbb{N}$) as the action of the operator $\mathcal{W}$. Let us call $\mathcal{W}_{\text{syn}}$ and $\mathcal{W}_{\text{seq}}$, respectively, the synchronous and the sequential version of $\mathcal{W}$, in the sense that $\mathcal{W}_{\text{syn}}$ invokes for displacement all the spheres satisfying $\xi'_j = 1$ independently, whereas $\mathcal{W}_{\text{seq}}$ assumes the sphere displacements to be dependent and therefore invokes the jumping spheres in sequence. The structure of $\mathcal{W}_{\text{syn}}$ is especially simple:

$$\mathcal{W}_{\text{syn}} : \begin{cases} \mathbf{r}_j \mapsto \mathbf{s}_j = \mathbf{a}_\nu^{(j)} \text{ with probability } p_\nu^{(j)}, & \forall j : \xi'_j = 1 \\ \mathbf{r}_j \mapsto \mathbf{s}_j = \mathbf{r}_j, & \forall j : \xi'_j = 0 \end{cases}, \tag{11}$$

where $\mathbf{s}_j$ is the new position of sphere j (the whole new configuration is denoted $\mathbf{S} = \{\mathbf{s}_1, \ldots, \mathbf{s}_N\}$), and is appropriate only if the cell neighborhood is of the Moore type, which ensures that no overlap will ever occur between two jumping spheres.

When the Von Neumann cell neighborhood is used instead, overlappings can result among two or more jumping spheres. Therefore, a sequential version of the operator $\mathcal{W}_{\text{seq}}$ must be adopted instead of $\mathcal{W}_{\text{syn}}$. This can be seen clearly from Fig. 1(c): Let us assume that the jumping sphere, starting from the boundary site (in yellow) between cells $\mathbf{c}_8$ and $\mathbf{c}_{13}$, selects a location close to the upper-left corner of cell $\mathbf{c}_{13}$ as outcoming position. If at the same time a jumping sphere in the boundary site between cells $\mathbf{c}_{17}$ and $\mathbf{c}_{22}$ points to a location close to the lower-right corner of cell $\mathbf{c}_{17}$, the result is an overlap between the two jumping sphere. In order to avoid overlaps, the choice of the lattice site $\mathbf{a}_\nu^{(j)}$ with probability $p_\nu^{(j)}$ is to be considered only as a biased trial move, where the bias lies in excluding all the outcoming position of sphere j that can cause overlap with the resting spheres, and the actual configuration updating must be sequential: $\mathcal{W}_{\text{seq}}$ prescribes that the sequence with which we invoke the jumping spheres is randomized, that the jumps are performed according to the randomized sequence, and that every one of such jumps is allowed only if it does not cause any overlap. Even though the configuration updating is sequential, the biasing procedure during which we exclude any possible overlap with the resting sphere *is still performed with full independence, i.e., synchronously*.

In brief, the transformation from configuration $\mathbf{R}$ to configuration $\mathbf{S}$, which can be written as $\mathbf{R} \to \mathbf{I} \to \mathbf{S}$, can be summarized as

$$\mathbf{S} = \mathcal{W} \circ \mathcal{D} \circ \mathcal{I} \circ \mathbf{R}, \tag{12}$$

where every operation is synchronous made exception for the last one, $\mathcal{W}$, which is synchronous if $\mathcal{W}_{\text{sync}}$ is used (in this case the Moore neighborhood is adopted for the cell connections) or is partially synchronous if $\mathcal{W}_{\text{seq}}$ is used (in this case the Von Neumann neighborhood is chosen).

Verifying that detailed balance is satisfied is straightforward: $p(\mathbf{I}|\mathbf{S})$ is given in Eq. (6), $\mathbf{I} \to \mathbf{I}'$ is deterministic [i.e., $p(\mathbf{I}'|\mathbf{I}) = 1$]. When $\mathcal{W}_{\text{sync}}$ is used, due to the randomization of the lattice sites we described above, a given set of lattices $\mathcal{A}^{(j)}$ (for all the j such that $\xi'_j = 1$) has the same probability of being constructed in both the processes $\mathbf{R} \to \mathbf{I} \to \mathbf{S}$ and $\mathbf{S} \to \mathbf{I} \to \mathbf{R}$. If the lattices $\mathcal{A}^{(j)}$ are the same in both the forward and the reverse transformations, as a consequence the distributions $p_v^{(j)}$ are the same as well, and detailed balance is obeyed.

When $\mathcal{W}_{\text{seq}}$ is used instead, the probability of picking a certain sequence with which the spheres are invoked to jump is equal to the probability of picking exactly the reversed sequence. When we reverse the sequence of jumps, every jumping sphere experiences the same scenario it experienced in the "forward" sequence, thus the resulting $\mathcal{A}^{(j)}$ lattices and $p_v^{(j)}$ distributions are also the same as in the forward sequence and detailed balance is obeyed.

V. NUMERICAL SIMULATIONS

We performed numerical runs of the simulation model over a system of size $L = 49.70$ Å, for values of the packing fraction, defined as $\eta = \pi N \sigma^3/6V$ (where N is the number of spheres, σ their diameter, and $V = L^3$ the volume), ranging from $\eta = 0.035$ to $\eta = 0.492$, i.e., covering the isotropic liquid region (the freezing point is located around $\eta = 0.494$). We fixed the sphere diameter to the value of $\sigma = 3.72$ Å. Consequently, the number N of hard spheres ranged between 240 and 2 240. The finer lattices were set according to a value of the parameter M equal to 10. The number of MC iterations was set to 10^7 steps (10^8 for the cases with $N = 2\,080$ and $N = 2\,240$). The simulations differed in the value assigned to the probability parameter, γ (described in Sec. IV), and in the number of cells per side, z (described in Sec. II), and in the use of the Moore or the Von Neumann neighborhoods (see Secs. II and III).

In order to describe how the model works, we need to properly define a quantity that can be taken as a measure of the average displacement acceptance. In general, the notion of acceptance as meant for traditional importance sampling MC schemes (i.e., the number of successful displacements divided by the number of displacement attempts) cannot be applied straightforwardly in the present model. This is because at each MC iteration the relative success of two collective operations, namely $\mathcal{D} \circ \mathcal{I}$ (in the present context we consider the application of $\mathcal{I}$ followed by $\mathcal{D}$ as a unique operation) and $\mathcal{W}$, must be taken into consideration. Let us then introduce first the quantity N_D^k, with $k = 1, \ldots, N_{\text{steps}}$, to represent the number of hard spheres that, after the application of the operation $\mathcal{D}$ at each MC iteration, occupy boundary sites (such spheres are the ones which can actually attempt a displacement), and the quantity N_{jump}^k, with $k = 1, \ldots, N_{\text{steps}}$, to represent the number of hard spheres that, at each MC iteration, actually perform a non-null displacement. Then we define the acceptance at iteration k as

$$J_{\text{acc}}^k = \begin{cases} N_{\text{jump}}^k / N_D^k & \text{if } N_D^k > 0 \\ 0 & \text{if } N_D^k = 0 \end{cases}, \tag{13}$$

and the average acceptance as

$$\langle J_{\text{acc}} \rangle = \frac{1}{N_{\text{steps}}} \sum_{k=1}^{N_{\text{steps}}} J_{\text{acc}}^k. \tag{14}$$

In Fig. 2(a) the average acceptance is plotted versus the total number of spheres when $\mathcal{W}_{\text{sync}}$ is used (together with the Moore neighborhood). The quantity $\langle J_{\text{acc}} \rangle$ gives the probability of any displacement to happen at each iteration. To complete the description of the model behavior under different parametrizations, we show in Fig. 2(b) the average number of jump attempts. Both the quantities $\langle J_{\text{acc}} \rangle$ and $\langle N_D \rangle$ need to be looked at in order to get a complete scenario.

When $\mathcal{W}_{\text{sync}}$ is used (together with the Moore neighborhood), we found that low values of γ are not recommended, since such conditions cause a high number of spheres to attempt a jump at each MC iteration. This, in turn, causes a high probability of boundary conflicts to be solved by the deterministic operator $\mathcal{D}$, which results in a low number of *actually moving* spheres—we recall that at each MC step, say the kth, the operator $\mathcal{D}$ forces the conflicting spheres at the

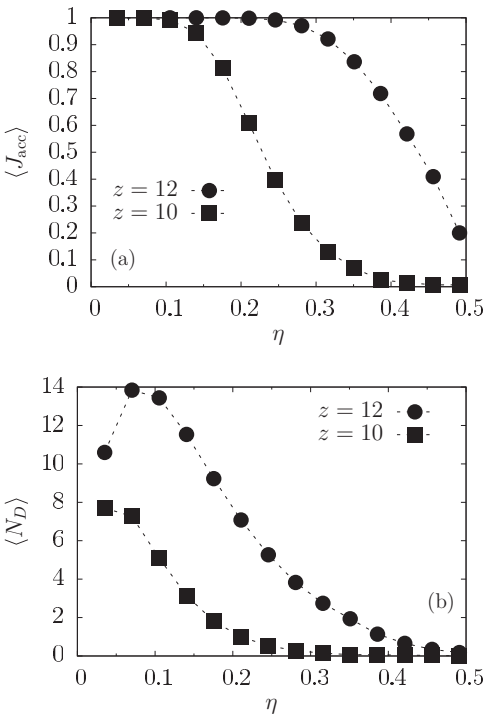

FIG. 2. (a) The jump acceptance and (b) the average number of jump attempts when the Moore neighborhood is used, for $\gamma = 0.9$ and for two different values of the number of cells per side; i.e., $z = 12$ and 10, corresponding, respectively, to $\ell \approx 4.17$ and $\ell = 5.0$.

boundaries to return back to their original positions, so that only the nonconflicting spheres at the boundary nodes, N_D^k in number, can actually keep their boundary position, thus having the chance to actually move. In fact, for low-intermediate values of γ we found (not shown) that the quantity $\langle J_{\rm acc}\rangle$ decays very rapidly with the number of particles (for $\gamma = 0.5$ and $\gamma = 0.1$ it reaches zero value at $\eta \approx 0.17$ and $\eta \approx 0.12$, respectively). In agreement with such considerations, we obtained the best $\langle J_{\rm acc}\rangle$ and $\langle N_D\rangle$ trends through high values of γ and z, more specifically $\gamma = 0.9$ and $z = 12$ [see Figs. 2(a) and 2(b)]. Intuitively, a higher number of cells (i.e., higher z) corresponds to a higher number of boundaries, which in turn implies a higher number of jump attempts. This, together with a high value of γ, which reduces the probability of conflicts at the boundaries, is expected to produce higher values of both the acceptance, $\langle J_{\rm acc}\rangle$, and the average number of displacements per MC step, $\langle N_D\rangle$. Such expectation is confirmed by the curves reported in Figs. 2(a) and 2(b). In particular, in Fig. 2(b) we can see that after an initial increase in $\langle N_D\rangle$ due to the increase in the number of spheres accessing the boundary sites, a certain loading is reached above which the number of spheres accessing the boundary sites during operation $\mathcal{I}$ is large enough to cause a higher number of conflicts to occur, which are solved by operator $\mathcal{D}$ through the cancellation of more displacement attempts.

As we can see from Figs. 3(a) and 3(b), when the $\mathcal{W}_{\rm seq}$ is used (together with the Von Neumann neighborhood) the curves of $\langle J_{\rm acc}\rangle$ and $\langle N_D\rangle$ change substantially. With respect to the Moore neighborhood, the use of the Von Neumann neighborhood causes much less conflicts to be solved by $\mathcal{D}$,

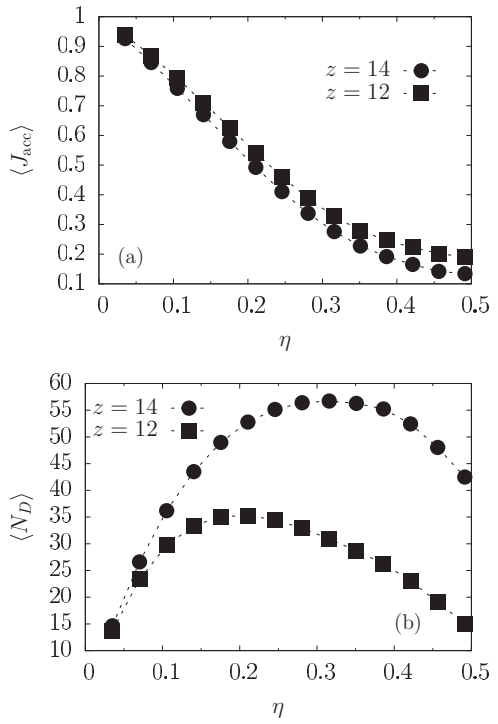

FIG. 3. (a) The jump acceptance and (b) the average number of jump attempts when the Von Neumann neighborhood is used, for $\gamma = 0.9$ and for two different values of the number of cells per side; i.e., $z = 14$ (a) and 12 (b), corresponding, respectively, to $\ell \approx 3.57$ and $\ell \approx 4.17$.

and the unsolved conflicts to contribute to lower the average acceptance—we remind that in such a case some jump attempts may fail due to superposition with spheres located at the corner cells as described in Sec. IV. This is the reason why the curve of $\langle J_{\rm acc}\rangle$ versus η starts decreasing immediately (i.e., it decreases with increasing hindering). At low loadings, $\langle J_{\rm acc}\rangle$ decreases approximately in the same way for all values of γ, then (not shown) more steeply for low γ because at higher loadings too many spheres attempt a jump and this fact, combined to the hindering effect of the moving particles with spheres at the corners, causes the average acceptance to fall rapidly. In Fig. 3(b), we can see that all the curves can be described analogously to what we did for Fig. 2(b), that is, a maximum of $\langle N_D\rangle$ is reached at a certain loading, which in the present case moves to higher values than the Moore neighborhood case. Again, this is a consequence of the fact that the use of the Von Neumann neighborhood causes much less conflicts to be solved by $\mathcal{D}$. Accordingly, in all the cases the number $\langle N_D\rangle$ is itself much higher than with the Moore neighborhood. The restraint imposed to the number of spheres to keep their position in the boundary sites is much weaker in the Von Neumann case, and the shape of $\langle N_D\rangle$ as a function of η shown in Figs. 3(b) and 2(b) is to be considered quite peculiar of the two different cell connectivities. However, for the lowest packing fractions (i.e., $\eta = 0.035$ and $\eta = 0.070$) we found that (not shown) lower values of γ cause a gain in the value of $\langle N_D\rangle$. These are the only cases in which a lower value of γ is to be preferred. This is due to the much more open structure of the Von Neumann neighborhood, where low values of γ at low loadings can still give rise to an acceptable number of actually moving particles. However, increasing η above 0.070 with low values of γ gives rise to an increasing number of conflicts, thus causing acceptance and number of actually moving spheres to fall rapidly to zero.

An important remark needs to be done about z, on which the number of cells of the lattice $\mathcal{L}$ depends. Again, higher values of z give higher values of $\langle N_D\rangle$, but the most important fact is that, once we relax the feature of full synchronicity of operator $\mathcal{W}$, it is possible to carry simulations where $\ell < \sigma$. This is the case for $z = 14$ [see Figs. 3(a) and 3(b)], a parametrization that is feasible only with $\mathcal{W}_{\rm seq}$ and is not applicable to the case of $\mathcal{W}_{\rm sync}$ used together with the Moore neighborhood, since this would cause unavoidable overlaps and the sphere displacements would be no longer independent.

In all cases, the acceptance and the average number of invoked particles reach low values when the loading is high. Observation of Figs. 2 and 3 suggests that our simulation method is not appropriate above the freezing point (i.e., for $\eta \geqslant 0.494$), since for high loadings the number of generated moves appears too low to ensure an accurate sampling. Different synchronous simulation strategies must be devised to explore the properties of the hard sphere system for packing fractions above the freezing point. However, below the freezing point, even in the case where the average acceptance and the number of attempted moves reach relatively low values, we found our sampling algorithms to provide reasonably accurate data. In Figs. 4(a) and 4(b) we compare the radial distribution functions, $g(r)$, obtained when $\mathcal{W}_{\rm sync}$ is used (analogous results are found when $\mathcal{W}_{\rm seq}$ is used instead) with the $g(r)$ obtained through standard MC for the isotropic liquid phase. As one

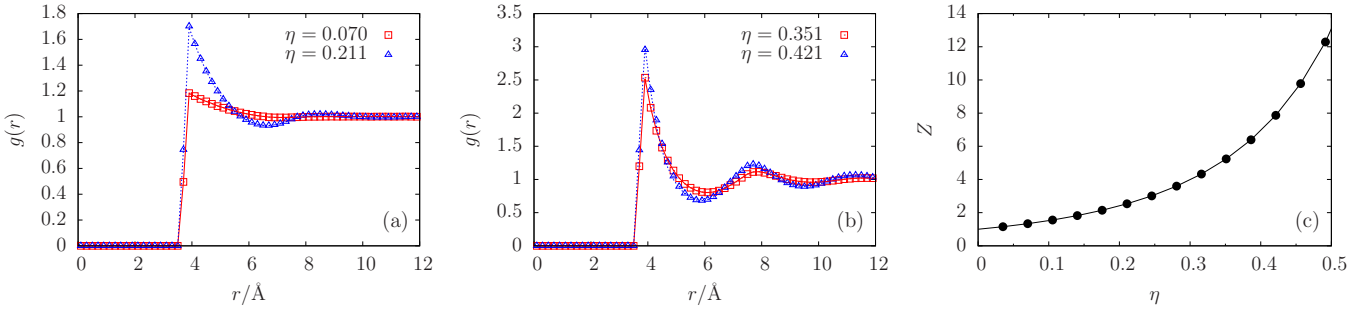

FIG. 4. (Color online) (a) and (b) are radial distribution functions at various values of the packing fraction, η, for a system simulated through the synchronous MC sampling with parameters $\gamma = 0.9$ and $z = 12$ (symbols), compared with the curves obtained through standard MC runs (lines). In (a) the solid and the dotted line refer to $\eta = 0.070$ and $\eta = 0.211$, respectively. In (b) the solid and the dotted line refer to $\eta = 0.351$ and $\eta = 0.421$, respectively. In (c) we show compressibility factors (dots) compared with the curve obtained through the Carnahan-Starling equation for the same systems (solid line).

can see, the agreement is excellent although the average acceptance is significantly less than in the lower loadings case. We calculated also the compressibility factor, defined through the virial theorem as [3]

$$Z = \frac{pV}{Nk_BT} = 1 + \frac{2\pi\sigma^3 N}{3V} \lim_{r\to\sigma^+} g(r), \tag{15}$$

where k_B is the Boltzmann factor and T the temperature. In our calculations, we approximated the limiting value of the radial distribution function at $r \to \sigma^+$ with $g(\sigma^+) \approx g(\sigma + 5 \times 10^{-3}$ Å). We compared the results with the Carnahan-Starling equation of state [18]:

$$Z = \frac{1 + \eta + \eta^2 - \eta^3}{(1-\eta)^3}. \tag{16}$$

Such comparison is shown in Fig. 4(c) for the case of $\mathcal{W}_{\text{sync}}$ with $\gamma = 0.9$ and $z = 12$ (an equivalent behavior was found for the case, not shown, of $\mathcal{W}_{\text{seq}}$ with $\gamma = 0.9$ and $z = 14$). The good agreement confirms that, in the range of loadings investigated, the accuracy of the sampling is good despite the low average acceptance rates at $\eta \geqslant 0.421$.

We also tested the sampling through the operator $\mathcal{W}_{\text{sync}}$ to the stationary source-sink problem applied to the case of hard disks migrating on a plane from a reservoir of length 20 Å to a sink located at the distance of 80 Å from the right end of the reservoir. The size of the system under consideration was of 100 Å along the x direction (reservoir included) and 50 Å along the y direction. We constructed the lattice of cells by partitioning the system into squares of side 3.125 Å and performed the simulation with probability parameter equal to $\gamma = 0.9$. We found that in the present application, where we used the Moore neighborhood together with the operator $\mathcal{W}_{\text{sync}}$, such value of γ ensures a good value of the average number of simultaneously moving disks per step (approximately 5%). The reservoir was constantly filled with disks through random insertions in such a way as to maintain an approximately constant packing fraction of 0.5. The disks were allowed to move without any directional bias throughout the plane. Moves to positions with $x < 0$ were always rejected, whereas moves beyond the right boundary of the system (i.e., positions with $x > 100$ Å) were interpreted as disk deletions. During their random motion throughout the system, no directional bias was applied. 10^6 steps were given to the system to converge to the stationary distribution, which was then sampled for the next 10^6 steps. The system was subdivided in slices 3 Å thick along the x axis, and data were collected for the quantity $\tilde{\eta}(x)$, an approximate measure of the packing fraction in every slice, defined as the average number of disk centers falling within each slice multiplied by the factor $\pi\sigma^2/4A$, where $A = 3 \times 50$ Å^2 is the area of a single slice. The simulation was replicated 50 times starting from slightly different initial conditions (namely, different values of the seed of the random number generator), and the stationary distributions were averaged together to give the profile reported in Fig. 5, along with results from standard MC simulations performed with the same criteria described above. Expectedly, the results show a trend which is an approximately linear decreasing function of the distance x from the reservoir. The satisfactory agreement between the two curves reported in Fig. 5 suggests that the synchronous algorithm described here could be used successfully in both equilibrium and nonequilibrium applications involving hard spheres (or hard disks).

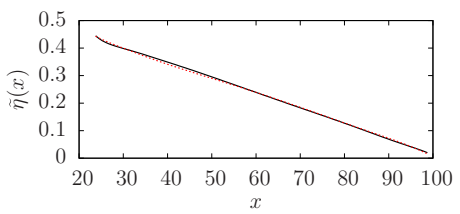

FIG. 5. (Color online) Stationary distribution for the source-sink problem applied to the case of hard disks. The solid and the dotted lines refer to the case of synchronous MC and standard MC, respectively.

VI. CONCLUSIONS

We developed a Monte Carlo algorithm for hard-sphere systems that contains elements of synchronicity that can be exploited in parallel computation. The method works by means of a sequence of operations, some of which require space discretization and cellular automata updating rules, that (i) select (synchronously) which spheres will move at each

iteration, (ii) solve (synchronously) the possible conflicts, (iii) generates (synchronously) possible outcoming positions for all the moving spheres, and (iv) subsequently performs the selected displacements (synchronously or sequentially). Full synchronicity is reached when the Moore neighborhood is used, together with the condition that the sphere diameter be less than the side of a lattice cell. If the feature of full synchronicity is relaxed, i.e., if the final operation (i.e., the actual displacement performing operation $\mathcal{W}$) is performed sequentially, the side of the lattice cell has no restraints (even though ℓ not too less than σ is recommended, in order to lower the hindering effects), and the Von Neumann neighborhood can be used instead of the Moore neighborhood. In such a case, the number of displacements per time step increases significantly, but the feature of displacement independence of the operation $\mathcal{W}$ is lost. However, even in the latter case, all the other operations (generation of the boundary configuration, resolution of conflicts, and biasing of the individual displacements) are still synchronous. We tested the algorithm to packing fractions in the range $0 < \eta < 0.494$, obtaining radial distribution functions in agreement with the ones obtained by standard MC simulations, and compressibility factors in agreement with the Carnahan-Starling equation. Finally, we applied the synchronous algorithm to the stationary source-sink problem finding a good agreement between the stationary distribution obtained by the synchronous algorithm and the one obtained through standard MC sampling. Although the applicability of the sampling criteria illustrated in the present work is restricted to the isotropic liquid phase only—at higher loadings the rejectance and the average number of moves are too low to ensure an accurate sampling, thus a different sampling algorithm must be devised to efficiently simulate the metastable liquid phase—we believe this model to be the first step toward the development of novel routes to introduce the feature of synchronicity in MC simulations, by suitably embedding cellular automata rules into off-lattice MC algorithms.

ACKNOWLEDGMENTS

The present work was produced within the research project "Progettazione su calcolatore di materiali avanzati per la rimozione e l'immagazzinamento della CO_2," developed at Università degli Studi di Sassari by means of the Contract "Ricercatore a Tempo Determinato" financed through the resources of POR Sardegna FSE 2007/2013–Obiettivo competitività regionale e occupazione, Asse IV Capitale umano, Linea di Attività l.3.1.

[1] B. J. Alder and T. E. Wainwright, Phys. Rev. **127**, 359 (1962).
[2] B. J. Alder and T. E. Wainwright, Phys. Rev. A **1**, 18 (1970).
[3] D. A. McQuarrie, *Statistical Mechanics*, 1st ed. (Harper and Row, New York, 1976).
[4] N. Metropolis, A. W. Rosenbluth, M. N. Rosenbluth, A. H. Teller, and E. Teller, J. Chem. Phys. **21**, 1087 (1953).
[5] B. J. Alder and T. E. Wainwright, J. Chem. Phys. **27**, 1208 (1957).
[6] C. Dress and W. Krauth, J. Phys. A **28**, L597 (1995).
[7] A. Jaster, Physica A **264**, 134 (1999).
[8] E. P. Bernard, W. Krauth, and D. B. Wilson, Phys. Rev. E **80**, 056704 (2009).
[9] J. A. Anderson, E. Jankowski, T. L. Grubb, and M. Engel, J. Comp. Phys. **254**, 27 (2013).
[10] S. Wolfram, Rev. Modern Phys. **55**, 601 (1983).
[11] B. Chopard and M. Droz, *Cellular Automata Modeling of Physical Systems*, 1st ed. (Cambridge University Press, Cambridge, England, 1998).
[12] J. Lebowitz, C. Maes, and E. R. Speer, J. Stat. Phys. **59**, 117 (1990).
[13] J.-P. Rivet and J. P. Boon, *Lattice Gas Hydrodynamics*, 1st ed. (Cambridge University Press, Cambridge, England, 2001).
[14] D. Dab, A. T. Lawniczak, J. P. Boon, and R. Kapral, Phys. Rev. Lett. **64**, 2462 (1990).
[15] A. Malevanets and R. Kapral, J. Chem. Phys. **110**, 8605 (1999).
[16] F. G. Pazzona, P. Demontis, and G. B. Suffritti, Phys. Rev. E **87**, 063306 (2013).
[17] F. G. Pazzona, P. Demontis, and G. B. Suffritti, Phys. Rev. E **88**, 062114 (2013).
[18] N. F. Carnahan and K. E. Starling, J. Chem. Phys. **51**, 635 (1969).